

Establishing an accurate depth-scale calibration in the top few nanometers of an ultrashallow implant profile

M. G. Dowsett,¹ S. H. Al-Harhi,^{1*} T. J. Ormsby,¹ B. Guzmán,² F. S. Gard,¹ T. C. Q. Noakes,³ P. Bailey,³ and C. F. McConville^{1,†}

¹*Department of Physics, University of Warwick, Coventry CV4 7AL, United Kingdom*

²*Dpto. Tecnología Electrónica, Universidad Politécnica de Madrid, Spain*

³*CLRC Daresbury Laboratory, Daresbury, Warrington Cheshire WA4 4AD, United Kingdom*

(Received 24 September 2001; published 7 March 2002)

A method to accurately determine the sputter yield of the matrix from the earliest stages of a sputter profile is described. Using the technique of medium-energy ion-scattering spectroscopy, this method provides data that enable a depth scale to be established from subnanometer depths onward. It may be adapted to samples containing a thin amorphous surface layer (e.g., a preamorphized shallow implant) or to crystalline surfaces containing a heavy-element marker layer. In this Brief Report we have used this method to interpret the near-surface profile using erosion-rate data obtained from a 1-keV boron implant into a germanium preamorphized silicon (001) surface.

DOI: 10.1103/PhysRevB.65.113412

PACS number(s): 68.35.Dv, 68.49.Sf, 68.55.Ln, 82.80.Ms

The development of methods for precise investigation and control of the physical and chemical state of the top few nanometers of a solid is becoming crucial to many areas of science and technology, notably semiconductor research and development. Sputter profiling using secondary ion-mass spectrometry (SIMS) is now widely used in the measurement of ultrashallow chemical composition, but interpretation of such data remains difficult because of the lack of a steady state in the primary ion-solid interaction across a significant part of the near-surface region. It is well known, for example, that the erosion rate of a material varies in the first few nanometers of a sputter profile (the transient region), and is highly dependent on the specific analysis conditions.^{1,2} Although low probe energies are mandatory for high depth resolution,³ it has been predicted that the difference between the surface and bulk yields increases as the incident probe energy is reduced.¹ Moreover, even if incident beam energies as low as 100 eV are used for sputtering, a significant fraction of the dopant in prospective device processes lies in the transient region.⁴ If, as is usually the case, the profile is quantified using a constant erosion rate derived from surface profilometer measurements, the near surface region will be distorted and the rest of the profile will be shifted accordingly.¹ For crater depths of less than 10 nm, it is not possible to use a surface profilometer to obtain the erosion rate accurately, and in any case the depth measured may contain a significant (but impossible to measure⁵) contribution from swelling as a result of implanted probe atoms.⁶ In fact the measurement does *not* correspond to the eroded depth in the matrix material. Ideally, it is the thickness of the matrix eroded per unit SIMS primary ion dose, which is required for accurate depth-scale calibration, and in this letter we report a method using medium-energy ion scattering (MEIS) for measuring this quantity directly.

We exploit the ability of MEIS to measure damage levels using the blocking of channels in a single crystal with an amorphized surface, and examine the rate of change of the residual damage in a preamorphized sample as a result of subsequent sputtering at sub-keV SIMS primary energies.⁷

The samples used in this study were cleaved from a Si(001) wafer preamorphized by a dose of $\sim 1 \times 10^{15} \text{ cm}^{-2}$ of germanium at 5 keV and implanted with a 1 keV boron dose of $5 \times 10^{14} \text{ cm}^{-2}$ (courtesy of Applied Implant Technology Ltd., UK). Part of the same wafer was capped with a ~ 15 nm amorphous silicon layer by UHV deposition at room temperature in a VG V90S molecular-beam-epitaxy (MBE) system. Hence, the same boron distribution was buried in some of the samples so that the distribution could be measured both with and without the influence of the transient effects normally observed in a SIMS profile. The sample preparation prior to the MEIS measurements was performed on several $\sim 1 \text{ cm}^2$ unannealed samples using the EVA 2000FL SIMS instrument at Warwick. To obtain measurements as a function of the incident-ion dose, each crater was individually prepared using a 500 eV O_2^+ primary beam at normal incidence with a crater size of 3 mm^2 with the ion doses in the range $4 \times 10^{15} - 2 \times 10^{17} \text{ O}_2^+ \text{ cm}^{-2}$. The $^{30}\text{Si}^+$, $^{11}\text{B}^+$, $^{74}\text{Ge}^+$, and $^{44}\text{SiO}^+$ secondary ion signals were all recorded to assess the correlation between ion-yield and sputter-yield steady-state doses.

MEIS saturated damage profiles were measured using 100-keV He^+ incident ions, with a total beam dose of $0.5 \times 10^{16} \text{ ions cm}^{-2}$. Experiments were performed using the double-alignment geometry of $[\bar{1}10]$ incidence and $[110]$ blocking, corresponding to incident and scattering angles of 45° and 90° , respectively. Each sample was studied in both channelled and random directions. The thickness of the damaged layer created by the 500 eV O_2^+ dose was well below the thickness of the Ge preamorphized layer, and so for the equilibrium dose regime ($< 3 \times 10^{16} \text{ cm}^{-2}$), sputtering the amorphous surface removes features due to damage from the original pre-amorphization. The method described here uses MEIS information relating to the loss of matrix (Si) atoms during sputtering. It is therefore insensitive to the effects of air exposure between sputtering and *ex situ* transfer to the MEIS instrument (although further oxidation is unlikely to occur⁸ in any case).

MEIS measurements taken in a channeling direction provide the damage profiles from the amorphous layer. Bombardment with 500 eV O_2^+ at normal incidence and with ion

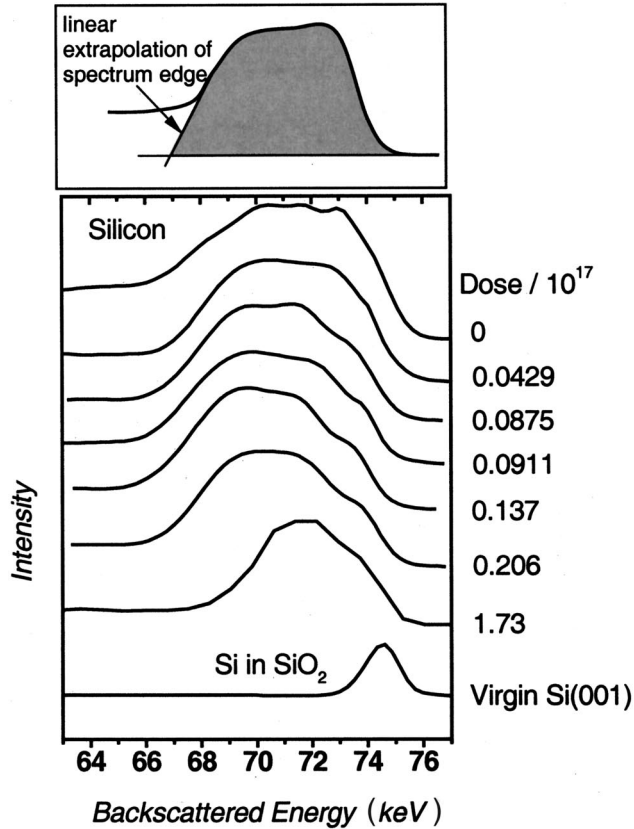


FIG. 1. MEIS channeling spectra of the Si peak and the effect of damage due to the 5 keV Ge and 1 keV B implants. The normally incident 500-eV O_2^+ ion doses are indicated and all the spectra were recorded with a 100-keV He^+ ion beam. Virgin Si(001) is also included for comparison. Shading on the inset indicates how the individual areas $A(\phi)$ were calculated.

doses in the range $1 \times 10^{15} - 2 \times 10^{17}$ ions cm^{-2} progressively removes the damage until the O_2^+ altered layer projects through the original amorphous/crystalline interface. The corresponding MEIS energy spectra are shown in Fig. 1. For the no-dose sample the thickness of the amorphized layer is 16.5 nm estimated at full width at half maximum measured using a stopping power of 200 eV/nm obtained from TRIM calculations. Detailed investigations show a high degree of damage from the surface to a depth of 13 nm with an average dechanneling χ_{min} value of 0.95 indicative of complete amorphization. The oxygen signal (not shown), due to the presence of the native- and sputter-beam-induced oxide, contributes to the shape of the high-energy edge of spectrum. Therefore, the transient investigations in this work start from the no-dose sample with SiO_2 on the surface, due to the native oxide, and end with the SiO_2 altered layer (possibly with an additional suboxide layer) formation due to the implanted primary oxygen atoms. The native oxide was estimated to be ~ 1 nm thick from comparison with an unimplanted crystalline wafer.

With reference to Fig. 1, the area $A(\phi)$ under each MEIS damage spectrum is first calculated, where ϕ is the ion dose. The dechanneling background in the crystalline material does not affect the intensity in the amorphized layer and hence the areas are calculated without the background sub-

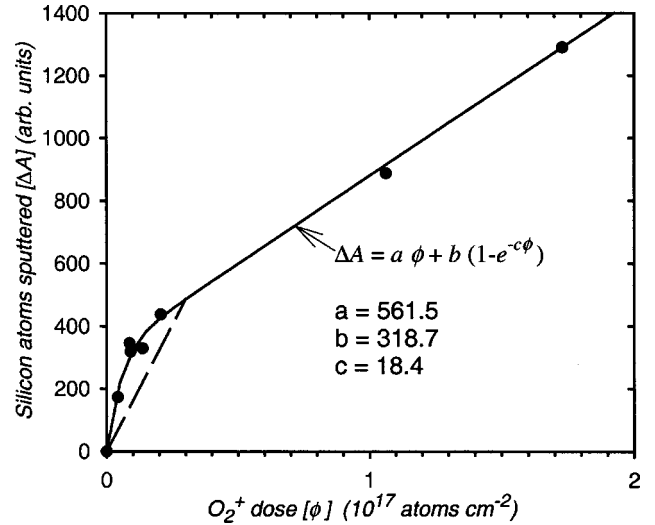


FIG. 2. A plot of the difference between area under the as-implanted damage profile and the oxygen-dosed profiles from the MEIS spectra as a function of oxygen dose. The fit shown was used in the SIMS-depth-profile correction.

traction, as shown. The difference in area $\Delta A(\phi)$ between each MEIS spectrum and the “no-dose” area A_0 is proportional to the total number of silicon atoms sputtered at that dose ϕ of O_2^+ ions, so that

$$\Delta A(\phi) = A_0 - A(\phi) \propto \int_0^\phi Y_{Si}(\phi) d\phi, \quad (1)$$

where Y_{Si} is the silicon sputtered yield.

Figure 2 shows the measured data for $\Delta A(\phi)$ as a function of ϕ (black circles). In principle, similar results could also be obtained for the erosion rate in a crystalline matrix sample, for example, with a SiGe, As, or Sb marker layer buried below a crystalline Si cap, by monitoring the energy shift with respect to the Si edge as the Si atoms in the cap are removed and accounting for the shift due to stopping by the oxygen from the SIMS beam. It is clear from Fig. 2 that the amount of eroded Si as a function of the bombardment dose initially increases nonlinearly as expected in the transient region. The data in Fig. 2 are well fitted by the function

$$\Delta A(\phi) = a\phi + b(1 - e^{-c\phi}), \quad (2)$$

whose slope is proportional to the sputter yield of the matrix. Fitting gives $a = 561.5$ (given the form of the equation, a is proportional to the bulk sputter yield Y_∞), $b = 318.7$, and $c = 18.35$, if ϕ is measured in units of $10^{17} O_2^+ cm^{-2}$. Previous measurements⁹ used the dose at which the silicon ion yield reached steady state as an estimate of the transient dose ϕ_{tr} , obtaining $\sim 1.5 \times 10^{16} O_2^+ cm^{-2}$ for silicon with an ~ 1 nm native oxide and $1.7 \times 10^{16} O_2^+ cm^{-2}$ for clean silicon. The sputter yield should also be in steady state by the end of the transient. The slope of Eq. (2) falls to within 5% of a at a dose of $3 \times 10^{16} O_2^+ cm^{-2}$, almost double that in the previous measurements. Referring for a moment to the dashed line in Fig. 3, which shows the boron SIMS profile for the uncapped sample analyzed under bombardment conditions identical to those calibrated by MEIS, one notes a spike at the surface, which is universally observed under all analyti-

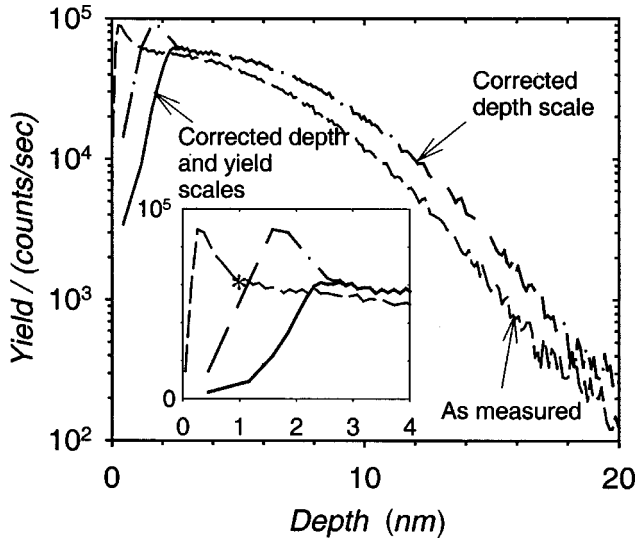


FIG. 3. Comparison between conventionally depth-calibrated (constant erosion rate from surface profilometer) boron profile using 500 eV O_2^+ at normal incidence, and profiles with corrected depth, along with both corrected depth and yield. The inset shows a linear plot of the top 4 nm.

cal conditions that produce a fully oxidized altered layer (i.e., near-normal incidence bombardment with O_2^+ or simultaneous use of oxygen flooding with more glancing-angle bombardment). The point marked by an asterisk—the end of the spike—corresponds to a dose of $3 \times 10^{16} O_2^+ cm^{-2}$. The boron spike was also observed in Ref. 9, flattening out at a similar dose. It appears that $3 \times 10^{16} O_2^+ cm^{-2}$ is a better estimate of ϕ_{tr} for 500 eV bombardment than obtained previously. Silicon-ion yields stabilize earlier because, after the initial steep rise, the increase in silicon ionization probability due to oxidation is compensated by the corresponding reduction in silicon partial sputter yield. (Similar arguments have been reported independently to account for the rapid stabilization of silicon-ion yields during sputtering with an oxygen jet¹⁰). It appears that boron-ion emission, in contrast, takes place at constant ionization probability α_B^+ , and therefore, after the initial steep rise (to the peak of the spike) its *ion yield* is proportional to the sputter rate of the matrix.

Previous experiments⁹ have also used the primary beam-energy-dependent shift (transient shift¹) to obtain the ratio of the average sputter yield $\langle Y_{Si} \rangle$ in the transient region to Y_∞ for 500 eV O_2^+ ions incident on (100) crystalline silicon. This average is important both as a check on the data and as a check on the depth scale which may be corrected in a simple way if it is known. The result was $\langle Y_{Si} \rangle / Y_\infty = 2.1$ for $\phi_{tr} \sim 1.7 \times 10^{16} cm^{-2}$, based on the assumption that the sputter yield equilibrated at the same dose as the ion yield. To obtain a comparison from Fig. 2, we note that $\langle Y_{Si} \rangle$ is proportional to the gradient of a straight line through the origin, intersecting the curve at $3 \times 10^{16} O_2^+ cm^{-2}$ (dashed line), and the resulting ratio $\langle Y_{Si} \rangle / Y_\infty$ is 2.9—somewhat higher than before. At present, there are relatively few data points in the $0.5 \times 10^{17} - 3 \times 10^{17} cm^{-2}$ dose range, which may result in some error. Nevertheless, the fact that the ion yields and the erosion rate stabilize at the same dose supports the estimate of ϕ_{tr} .

From Eq. (2) it follows that

$$\frac{Y_{Si}(0)}{Y_\infty} = \frac{1}{a} \left. \frac{d[\Delta A(\phi)]}{d\phi} \right|_{\phi=0}, \quad (3)$$

which, from the data in Fig. 2, gives a value of 11–12, rather larger than the predictions in Ref. 1, which yield a ratio of about 6.5. Taking a literature value of $Y_\infty = 0.14$ one gets a value in the range 1.5–1.7 Si/O_2^+ for the initial sputter yield.¹⁰ Unlike the sputter yield, the low-energy ion yield is close to zero at the surface. This implies that the high surface sputter yield is due to weak near-surface bonds, without significant polarization (since this would, in general, lead to high ion yields). Similar effects are observed in crystalline and amorphous silicon (as opposed to the amorphized silicon used here) so that the high concentration of Ge near the surface of this sample is unlikely to be affecting the data. Conversely, MEIS shows the top few nanometers to be composed of native oxide, which would ordinarily exhibit high positive-ion yields. One possible explanation of the phenomenon is that initially high top-monolayer concentrations of hydrogen undergo ion-impact-enhanced reaction with silicon to produce volatile silane, which carries silicon away from the surface by evaporation rather than sputtering.

The eroded depth of matrix z for a given dose ϕ is proportional to $\Delta A(\phi)$, and since

$$\lim_{\phi \rightarrow \infty} z = \phi Y_\infty \Omega_{Si}, \quad (4)$$

where Ω_{Si} is the atomic volume of the matrix, the constant of proportionality must be $Y_\infty \Omega_{Si} / a$ so that, in general,

$$z = 10^{17} \frac{Y_\infty}{a} \Omega_{Si} \Delta A(\phi) \text{ (}/cm), \quad (5)$$

where the factor of 10^{17} accounts for the dose scale used in the fitting of Eq. (2). In Eq. (5), z has units of centimeters if a is dimensionless and ΔA and b are in units of 10^{17} atoms cm^{-2} . Substituting $\Delta A(\phi_{tr} = 3 \times 10^{16}) = 486$ from Eq. (2) into Eq. (5), using the value 0.14 Si/O_2^+ ¹¹ for Y_∞ and taking $\Omega_{Si} = 2 \times 10^{-23} cm^3$ we find the width of the transient region (i.e., the thickness of silicon sputtered to achieve steady state) to be 2.4 nm, again higher than the figure of 0.7 nm estimated for crystalline Si .⁹

Equation (5) may be used to apply a fully corrected depth scale to an implant profile, either by calibrating the data using Y_∞ as above, or by using the measured crater depth z_{meas} and ϕ_{tot} to fix the end point for Eq. (2). Implicitly this gives the constant terms in Eq. (5), e.g.,

$$z = \frac{z_{meas}}{\Delta A(\phi_{tot})} \Delta A(\phi), \quad (6)$$

where it is assumed that z_{meas} is sufficiently large that errors due to the altered layer are insignificant. Returning to Fig. 3, the dash-dot line shows the profile with a depth scale deduced from Eq. (6) where $\phi_{tot} = 2.9 \times 10^{18} O_2^+ cm^{-2}$. The inset shows the near-surface behavior on a linear scale. (Primary ion current is 35 nA, bombarded area is $190 \mu m^2$, profile time is 4791 s.) The corrected profile is shifted by 1.4 nm, which is somewhat more than expected from transient shift data for crystalline silicon (0.9 nm keV^{-1} per O_2^+ ¹²).

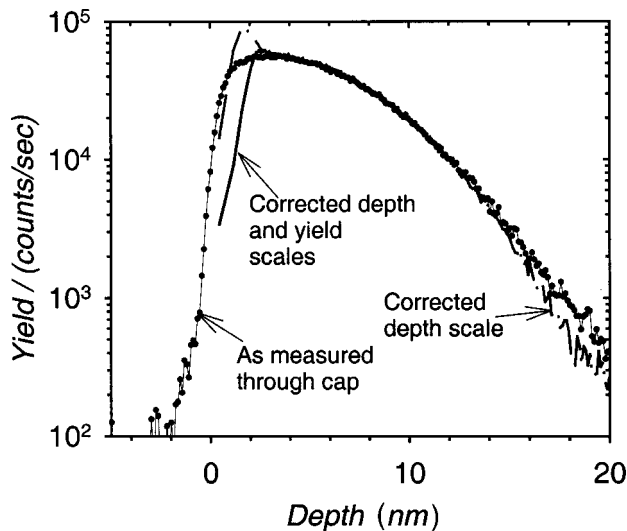


FIG. 4. Comparison between corrected and capped profiles. The depth scale of the capped profile has been offset by -15.3 nm (the thickness of the cap).

Note that the main effect of the correction has been to stretch the surface spike laterally. Comparison between the measured profile (dashed line) and the measured profile from the capped sample (dotted line in Fig. 4) lends further support to the notion that boron is sputtered out at constant α_B^+ in the spike.¹³ The measured dose ratio ($D_{uc/c}$) between the uncapped and capped samples is given by

$$D_{uc/c} = \frac{\sum_{\text{surface}}^{\text{profile end}} Y_{uc}}{\sum_{\text{interface}}^{\text{profile end}} Y_c}, \quad (7)$$

where Y_{uc} and Y_c are the $^{11}\text{B}^+$ yields in counts s^{-1} for the uncapped and capped samples, respectively. We find that $D_{uc/c} \sim 0.99$ so that the spike in the as-measured data conserves the boron dose as expected for constant α_B^+ . (Note that this dose ratio is absolute in the sense that it uses only

the raw data and requires no reference materials.) The decay slope on the spike should therefore be due to the decreasing erosion rate, while the rising slope at the very earliest stages of the profile occurs outside the constant-ionization regime. Consequently, the stretching process in the depth correction has not conserved the boron dose and we should apply an inverse correction to the boron-ion yield Y_B^+ ,

$$Y_{\text{corrB}}^+(\phi) = Y_B^+(\phi) \frac{Y_\infty}{Y_{\text{Si}}(\phi)}. \quad (8)$$

The results of this procedure are shown by the solid curve in Fig. 3. The boron-surface spike is now completely removed as one would expect for an ideal profile without transient effects. The capped sample, which is free from transient effects, provides a reference for the yield correction. The comparison in Fig. 4 between the dotted line (as measured through the cap) and the fully corrected profile shows that the yield correction works well in the decaying part of the spike, again supporting the hypothesis that boron is sputtered at constant yield in this region.

In summary, we have demonstrated an application of MEIS, which has been used directly to provide an accurate measurement of the dose-dependent sputter yield of silicon during the SIMS-surface transient regime. We have shown how these data may be used for profile correction in the increasingly important top few nanometers of an ultra-shallow implant profile and achieve quantitative agreement with other measurements. The suggestion, however, is that further use of this method should provide even more accurate depth scale by extending this type of measurement to other incident-ion energies and matrices (e.g. crystalline silicon) to fully exploit its potential.

Support for this research project from the following Companies and Institutions is gratefully acknowledged: The Engineering and Physical Sciences Research Council (EPSRC) of the UK. Applied Implant Technology Ltd., and Atomika Instruments GmbH.

*Present address: Department of Physics, Sultan Qaboos University, Muscat, P. O. Box 36, Code 123, Sultanate of Oman.

†Corresponding author. FAX: ++44-24-7669-2016. Email address: C.F.McConville@warwick.ac.uk

¹K. Wittmaack, *Philos. Trans. R. Soc. London, Ser. A* **354**, 2371 (1996).

²D. P. Chu, M. G. Dowsett, T. J. Ormsby, and G. A. Cooke, in *Characterization and Metrology for ULSI Technology*, edited by D. G. Seiler, *et al.* AIP Conf. Proc. **449** (AIP, Woodbury New York, 1998) p. 771.

³J. B. Clegg, N. S. Smith, M. G. Dowsett, M. J. J. Theunissen, and W. B. deBoer, *J. Vac. Sci. Technol. A* **14**, 2645 (1996).

⁴M. G. Dowsett, in *Proceedings of Atomic Level Characterizations for New Material and Devices 97*, edited by M. Yurimoto and S. Ichimura (Wiley, New York, 1997), p. 303.

⁵K. Wittmaack, M. Strigl, and A. Horwarth, *Surf. Interface Anal.* **29**, 717 (2000).

⁶D. S. Simons, in *Secondary Ion Mass Spectrometry SIMS*, edited by A. Bennighoven *et al.* (Wiley, New York, 1996) Vol. X, p. 76.

⁷M. G. Dowsett, C. Jeynes, E. A. Clark, R. Webb, and S. M. Newstead, *Secondary Ion Mass Spectrometry SIMS*, edited by A. Bennighoven *et al.* (Wiley, New York, 1990), Vol. VII, p. 615.

⁸M. G. Dowsett, S. B. Patel, and G. A. Cooke, *Secondary Ion Mass Spectrometry SIMS*, edited by A. Bennighoven *et al.* (Wiley, New York, 2000), Vol. XII, p. 85.

⁹M. G. Dowsett, T. J. Ormsby, D. I. Elliner, and G. A. Cooke, *Secondary Ion Mass Spectrometry SIMS*, edited by G. Gillen *et al.* (Wiley, New York, 1998), Vol. XI, p. 371.

¹⁰K. Wittmaack, *J. Vac. Sci. Technol. B* **16**, 2776 (1998).

¹¹N. S. Smith, M. G. Dowsett, B. McGregor, and P. Phillips, *Secondary Ion Mass Spectrometry SIMS*, edited by Werner *et al.* (Wiley, New York, 1996), Vol. X, p. 363.

¹²K. Wittmaack, *Surf. Interface Anal.* **24**, 389 (1996).

¹³M. G. Dowsett, J. Bellingham, S. H. Al-Harathi, B. Guzmàn, T. J. Ormsby, G. A. Cooke, and C. F. McConville, in *Proceedings of the 2nd International Symposium on SIMS and Related Techniques, 2000*, edited by M. Kudo, (Seikei University, Tokyo, Japan, 2000).